Electronic structure of the hydrogen-adsorbed $SrTiO_3$(001) surface studied by polarization-dependent photoemission spectroscopy

R. Yukawa,[1] S. Yamamoto,[1] K. Ozawa,[2] M. D'Angelo,[3] M. Ogawa,[1] M. G. Silly,[4] F. Sirotti,[4] and I. Matsuda[1,*]

[1]*Institute for Solid State Physics, the University of Tokyo, Kashiwa, Chiba 277-8581, Japan*

[2]*Department of Chemistry and Materials Science, Tokyo Institute of Technology, Meguro-ku, Tokyo 152-8551, Japan*

[3]*Institut des Nanosciences de Paris, Université Pierre et Marie Curie-Paris 6, CNRS-UMR 7588, 4 place Jussieu, 75252 Paris, France*

[4]*TEMPO Beamline, Synchrotron Soleil, L'Orme des Merisiers Saint-Aubin BP48 91192 Gif-sur-Yvette Cedex, France*

(Received 8 December 2012; published 25 March 2013)

The metallic band structure of the hydrogen-adsorbed $SrTiO_3$(001) surface is studied by polarization-dependent photoemission spectroscopy measurements. With the dipole-transition selection arguments, we attributed the metallic peaks into the Ti $3d_{xz}$, $3d_{yz}$, and $3d_{xy}$ bands. These t_{2g} bands are partially filled with electrons upon H-induced downward band bending at the surface. Energy splitting of the Ti $3d$ t_{2g} bands is considered to be induced by a quantum confinement along the surface normal (z) direction. The metallic peaks are accompanied by the incoherent states induced by many-body interactions, which likely indicates that the electronic system forms a two-dimensional liquid phase. Also emerged by H exposure are an in-gap state and a σ(O − H) state. The possible origin and the feature of these states are discussed from the polarization dependence of the photoemission intensity.

DOI: 10.1103/PhysRevB.87.115314 PACS number(s): 79.60.Dp, 73.20.−r, 71.30.+h

I. INTRODUCTION

Electronic systems at surfaces and interfaces of transition-metal oxides, such as $SrTiO_3$ (STO), have nowadays attracted intense interests for their promising technological applications in future electronics. For example, two-dimensional electron gas (2DEG), formed at an interface of $LaAlO_3$ and $SrTiO_3$ crystals, has shown a large carrier mobility and high magnetoresistance.[1–5] A photoemission research has observed the 2DEG also on a cleaved STO surface, which has opened its possible application as transparent devices.[6] Further photoemission experiments on a cleaved STO surface which is exposed to ultraviolet rays have shown that the 2DEG is rather described by the two-dimensional electron liquid (2DEL) because spectral features enhanced by strong electron correlations have been observed.[7] However, these 2D electrons at the interface and the surfaces have been considered to originate from oxygen vacancies, which may become fatal scatterers for conducting electrons. Recently, a well-defined STO(001) surface was found to become metallic by hydrogen adsorption through angle-resolved photoemission spectroscopy (ARPES) and surface transport measurements.[8] Surface metallization proceeds with appearance of the metallic peak, which accompanies a large spectral tail and an electronic state in the bulk band gap (in-gap state, IGS). Assignments of these photoemission features have been strongly requested for proper understandings of the 2D electronic systems at metal-oxide surfaces.

In this research, we have carried out photoemission spectroscopy measurements on the metallic H/STO surface to study details of the surface electronic structure. From the polarization dependence of the photoemission spectra, symmetric properties of the electronic states are determined. The metallic peaks and the spectral tails, having the same symmetry, are assigned to coherent and incoherent parts of the Ti $3d$ t_{2g} photoemission signal, respectively. The electronic system may form the 2DEL phase. Appearance of the IGS peak likely results from the O $2p$–Ti $3d$ hybridized states. From changes of the Ti, Sr, and O core-level spectra by hydrogen adsorption, the hydrogen atoms are found to adsorb on the oxygen sites. In addition, from the size of Fermi surface, a net amount of the transferred electrons from hydrogen to the surface is estimated.

II. EXPERIMENTS

The photoemission spectroscopy experiments were carried out at the TEMPO beamline in SOLEIL and at BL07LSU in SPring-8, where p- and s-polarized undulator beams were available. Details of the experimental stations are described elsewhere.[9–11] The measurements were made at 300 and 80 K under ultrahigh vacuum (UHV) condition with a base pressure of $< 4 \times 10^{-8}$ Pa.

In this research, n-type STO(001) wafers (0.05 wt% Nb-doped, PI-KEM Ltd., UK, and Shinkosha Co. Ltd., Japan) were used as samples. Before introducing the wafers into the UHV chambers, they were treated with buffered HF solution (pH $\sim$ 3.5) for 30 s, followed by rinsing with distilled water. This process has been known to leave the TiO_2-terminated surface.[12] Most of the previous photoemission researches on STO have been done on cleaved[6,7,13] or annealed[12,14–18] surfaces. However, cleavage and annealing of the STO samples in UHV chambers are considered to make oxygen vacancies on the surfaces.[6,19,20] In order to avoid the oxygen vacancies on the surface, a clean STO(001) surface was prepared by annealing at 600 °C under 6×10^{-4} Pa of oxygen gas (99.999% purity). An ordered surface was ascertained by observation of a sharp 1×1 pattern of low-energy electron diffraction. Negligible carbon contamination was ascertained by absence of the C $1s$ peak in the core-level photoemission. Adsorption of atomic hydrogen on the STO(001) surface was made at room temperature by cracking hydrogen molecules with a hot tungsten filament under the atmosphere of hydrogen gas; $P(H_2) = 1.5 \times 10^{-4}$ Pa. In order to prevent direct heating and contamination of the sample surface from the hot filament,

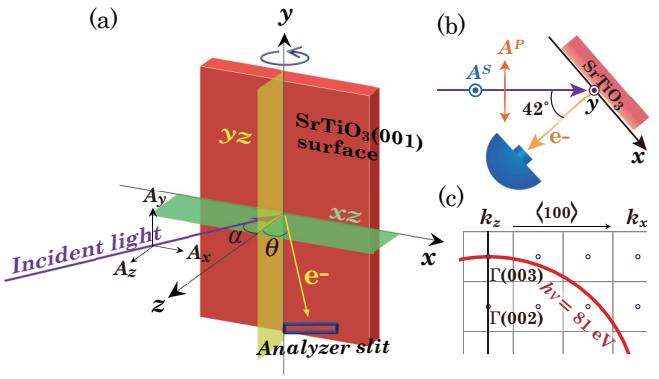

FIG. 1. (Color online) (a), (b) Schematic drawings of the experimental geometry with the light polarization vectors. The x,y,z axes are set parallel to the ⟨100⟩, ⟨010⟩, ⟨001⟩ directions of the STO crystal, respectively. Direction of the incidence light and the analyzer slit are in the xz mirror plane (green). Photoelectrons emitted in the yz mirror plane (yellow) are detected at the analyzer only at the normal emission ($\theta = 0^\circ$) position. The sum of the incidence angle α and the emission angle θ was fixed at 42°. (c) Schematic representation of Brillouin zones for the STO crystal in the ⟨100⟩-⟨001⟩ plane. Using an inner potential 12 eV measured from E_F (Ref. 14), a sphere of the final-state free electron at $h\nu = 81$ eV is obtained.

a shielding cover was mounted between the sample and the filament. During the hydrogen adsorption, temperature near the sample was monitored. Increase of the monitored temperature during the hydrogen dosage was less than 30 K. It should be noted that adsorption rate depends on the experimental chambers and, especially, on geometrical positions of the sample and the filament.

Measurement geometries for valence band photoemission spectroscopy are schematically shown in Figs. 1(a) and 1(b). With the orthogonal basis defined on a surface, a set of polarization vectors of the incident light is expressed as $\mathbf{A} = (A_x,\ A_y,\ A_z) = (A^p \cos\alpha,\ A^s,\ A^p \sin\alpha)$, where A^p and A^s correspond to the p- and s-polarization vectors, respectively. The angle α is referred from the surface normal. Recalling the dipole approximation for the photoemission process,[21] photoemission intensities taken with p-polarized (I^p) and s-polarized (I^s) photons, and the matrix element for the electron-photon interaction can be expressed as

$$I^{s,p} \propto \left|\langle \Psi_f | \mathbf{A}^{s,p}_{\rm pes} \cdot \nabla | \Psi_i \rangle\right|^2 A_{\rm spectral}, \qquad (1)$$

where $\mathbf{A}^s_{\rm pes}$ and $\mathbf{A}^p_{\rm pes}$ are vector potentials of the incident light described as $\mathbf{A}^{s,p} = \mathbf{A}^{s,p}_{\rm pes} e^{i(\omega t+\varphi)}$ with the phase shift φ. $|\Psi_i\rangle$ and $|\Psi_f\rangle$ are ket vectors in the initial and final states, respectively. The spectral function $A_{\rm spectral}$ contains coherent and incoherent parts of the photoemission process, which carries information on the many-body interactions of the probing electronic states.[22,23] Briefly, a peak and the accompanying spectral tails correspond to the coherent and incoherent parts, respectively. Appearance of the photoemission tail has been regarded as a signature of the large many-body interactions, such as those in a high-temperature superconductor.[24]

In the present measurement configuration, photoemission intensities with polarized light are expressed in terms of the matrix element as

$$I^p \propto \left|\langle \Psi_f | \mathbf{A}^p_{\rm pes} \cdot \nabla | \Psi_i \rangle\right|^2 = A^2 \left| \int_{-\infty}^{\infty} dx\ \Psi_f^*(x,y,z) \frac{\hbar}{i}\frac{\partial}{\partial x} \Psi_i(x,y,z) \cos\alpha + \int_{-\infty}^{\infty} dz\ \Psi_f^*(x,y,z) \frac{\hbar}{i}\frac{\partial}{\partial z} \Psi_i(x,y,z) \sin\alpha \right|^2, \qquad (2a)$$

$$I^s \propto \left|\langle \Psi_f | \mathbf{A}^s_{\rm pes} \cdot \nabla | \Psi_i \rangle\right|^2 = A^2 \left| \int_{-\infty}^{\infty} dy\ \Psi_f^*(x,y,z) \frac{\hbar}{i}\frac{\partial}{\partial y} \Psi_i(x,y,z) \right|^2, \qquad (2b)$$

where the photon intensities are normalized to $|\mathbf{A}^{s,p}|^2 = A^2$.

When one assumes that the initial states and the final states are isotropic along the x, y, and z directions, the intensity ratio becomes $I^p/I^s = (\cos\alpha + \sin\alpha)^2 \approx 2.0$ at the normal emission geometry ($\alpha = 42^\circ$ in the present measurement condition). It is noted that, considering the existence of refraction and reflection on the STO surface, A_z ($=A^p \sin\alpha$) should be weakened inside the bulk,[25] and therefore this intensity ratio would become smaller than the calculated value of 2. Thus, when the ratio is larger than 2, the state is considered to be mainly composed of the orbitals extending along the surface normal (the out-of-plane components). Similarly, if one assumes that the contribution to the matrix element from A_z is zero, the intensity ratio becomes $I^p/I^s = \cos^2\alpha \approx 0.55$. This simple analysis helps to assign anisotropy of an electronic state.

III. RESULTS AND DISCUSSION

Figure 2(a) shows normal emission angle-integrated spectra of the clean STO and H/STO surfaces taken with p- and

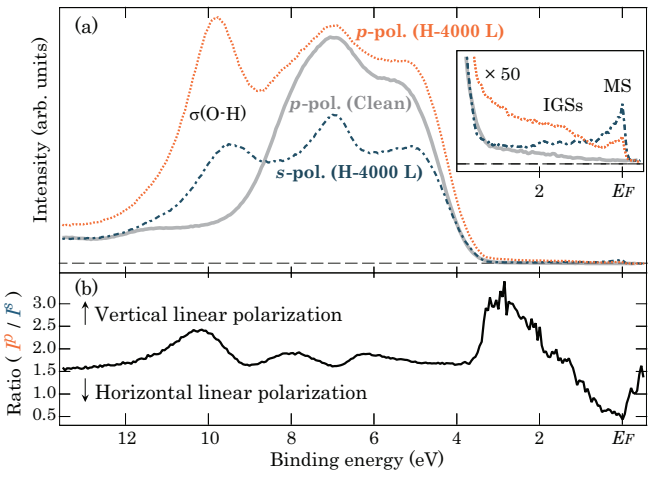

FIG. 2. (Color online) (a) Angle-integrated valence band spectra of the H-covered STO(001) surface measured at 80 K with p-polarized (orange dots) and s-polarized (blue dashed) light at $h\nu = 81$ eV. For comparisons, a spectrum of a clean STO(001) surface, taken at 300 K with p-polarized light, is shown (gray solid). The inset is magnified spectra near the Fermi level (E_F). (b) Intensity ratio of the H/STO spectra taken with p-polarized (I^p) and s-polarized (I^s) light.

s-polarized light and with a transmission mode of the analyzer. Surface metallization was achieved by the 4000 L H-dosage (1 L $= 1.3 \times 10^{-4}$ Pa s). The metallic band is observed at the photon energy of $h\nu = 81$ eV, which corresponds to the $\Gamma(003)$ point in the momentum as shown in Fig. 1(c). The spectra are normalized with the photon flux (a drain current of the focusing mirror in the beamline). On the clean STO surface, the energy region between the Fermi level and the O $2p$ band edge at the binding energy (E_B) of ~3 eV corresponds to the bulk band gap, and there is no spectral feature in this energy region. By dosing hydrogen atoms on the STO surface, there emerges a metallic state (MS) with a spectral tail at the Fermi level and the IGS at $E_B \sim 1.3$ eV. The spectral change indicates surface metallization, as reported previously.[8] Also, a peak appears at $E_B \sim 10$ eV by hydrogen adsorption. By annealing the H-dosed STO under oxygen gas, these peaks disappear and the peak positions of the core-level spectra shift back to the original values on the clean surface.

Figure 2(b) plots the photoemission intensity ratio I^p/I^s of the H/STO spectra taken by the different polarized light. In the present measurement configuration, shown in Fig. 1, $I^p/I^s \sim 2$ indicates that the electronic state is isotropic with respect to the out-of-plane and in-plane directions. The intensity ratio of both the MS peak and the spectral tail exhibit the in-plane character ($I^p/I^s < 1$). Thus, these spectral features have the same origin and can naturally be assigned to coherent and incoherent parts of A_{spectral} in Eq. (1). Clear appearance of the spectral tail, or the incoherent part, indicates strong electron correlations on the MS.[7,15] The MS band is likely assigned to the bulk conduction band of the Ti $3d$ t_{2g} orbitals that are partially filled with electrons at the H/STO surface.[8] The in-plane character of the MS band indicates that the Ti $3d$ t_{2g} band has the x or y component. On the other hand, the IGS peak seems isotropic and it is expected to have a different origin from the MS band as discussed below. A peak at $E_B \sim 10$ eV, appearing after the hydrogen dosage, is assigned to the σ(O-H) state.[16] The assignment is consistent with the change of the O $1s$ core-level peak, as will be described in Fig. 5. Enhancement of the photoemission intensity at 10.5 eV by the p-polarized light ($I^p/I^s > 2$) indicates that the O-H bond is along the surface-normal direction. According to the previous photoemission study on a dissociated H_2O on STO(001), the energy separation between σ(O-H) and π(O-H) states is 3.6 eV.[16] Thus, a small dip at $E_B \sim 7$ eV in Fig. 2(b) may be assigned to the π(O-H) state having the in-plane character. The intensity ratio of the dip ($I^p/I^s \sim 1.5$) is larger than the calculated ratio for the in-plane character ($I^p/I^s \sim 0.55$). This can be explained by the overlap of the isotropic O $2p$ states and the π(O-H) states at $E_B \sim 7$ eV. It is of note that adsorption of the hydrogen atoms on the oxygen sites has been predicted by the *ab initio* calculation.[26]

Around $E_B \sim 3$ eV, one notices that the I^p background intensity becomes large after the hydrogen adsorption and I^p/I^s is greater than 2, although there is no notable peak in the spectra [the inset of Fig. 2(a)]. The properties are similar to those of the surface photoemission (SP) effect,[27–29] which is neglected in the approximation of Eq. (2). Since SP is caused by the change of A_z by the difference of the permittivity between the vacuum and the sample surface, this emission is considered to be observable only by p-polarized

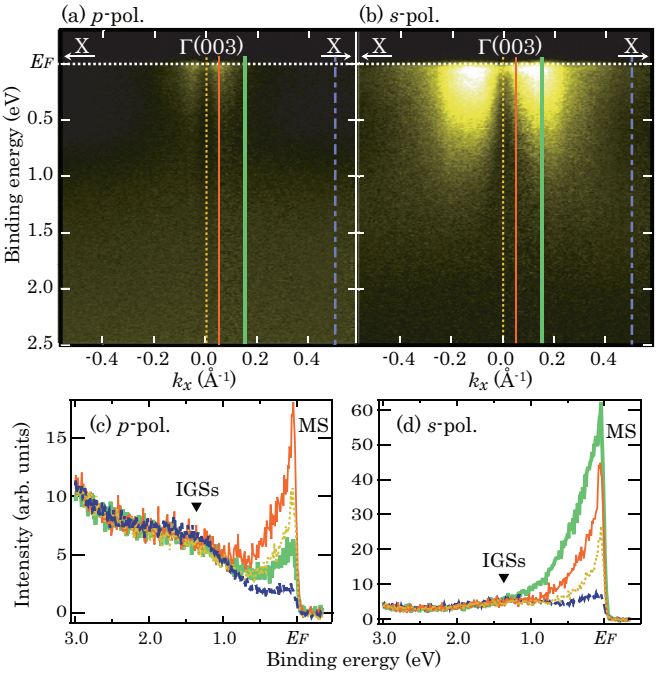

FIG. 3. (Color online) Photoemission intensity map of the 4000 L H-dosed STO(001) along the k_x direction. The data were taken at 80 K using p-polarized (a) and s-polarized (b) light at $h\nu = 81$ eV. The same color scales against the intensities are applied for both spectra. The energy distribution curves (EDCs) at $k_x = 0.00$, 0.05, 0.15, and 0.50 Å^{-1} are listed in (c) and (d), and their k_x positions are indicated on (a) and (b) as vertical lines. The characteristic humps are marked with black triangles. All spectra are normalized with the photon flux.

light. Thus, the spectral feature may tentatively be assigned to the SP channel, however, the further discussion is beyond the scope of this paper.

Figures 3(a) and 3(b) show ARPES data around $\Gamma(003)$ taken with (a) p-polarized and (b) s-polarized light with an angular mode of the analyzer. As described in Fig. 2, the MS has the in-plane character and, thus, it appears much clearer in the s-polarization geometry [Fig. 3(b)] than in the p-polarization case [Fig. 3(a)]. In both angle-resolved spectra in Fig. 3, the obvious MS peaks are identified at $k_x \sim 0.05$ Å^{-1} and $k_x \sim 0.15$ Å^{-1} for p- and s-polarized light, respectively, while the intensities become significantly weak at $k_x = 0$ Å^{-1}. The sharp intensity variation depending on k_x can be understood by symmetry arguments of the Ti $3d$ t_{2g} orbitals that contribute to the metallic band. To see the precise structure of the metallic band, the enlarged ARPES spectra are examined. Figure 4 shows that the metallic band is composed of several branches. In the spectra measured with the p-polarized light [Fig. 4(a)], a single branch is observed at just below the Fermi level ($E_B < 60$ meV) in a narrow k_x region. For the s polarization in Fig. 4(b), three branches are observable: one is located at $E_B < 60$ meV in a relatively wide k_x region, one shows rather large energy dispersion at $E_B < 120$ meV, and one also has large dispersion but is located at the deeper energies ($E_B \sim 200$ meV).

Relations between the symmetry of the Ti $3d$ t_{2g} orbitals (d_{xy}, d_{xz}, and d_{yz}) and the measurement geometry are

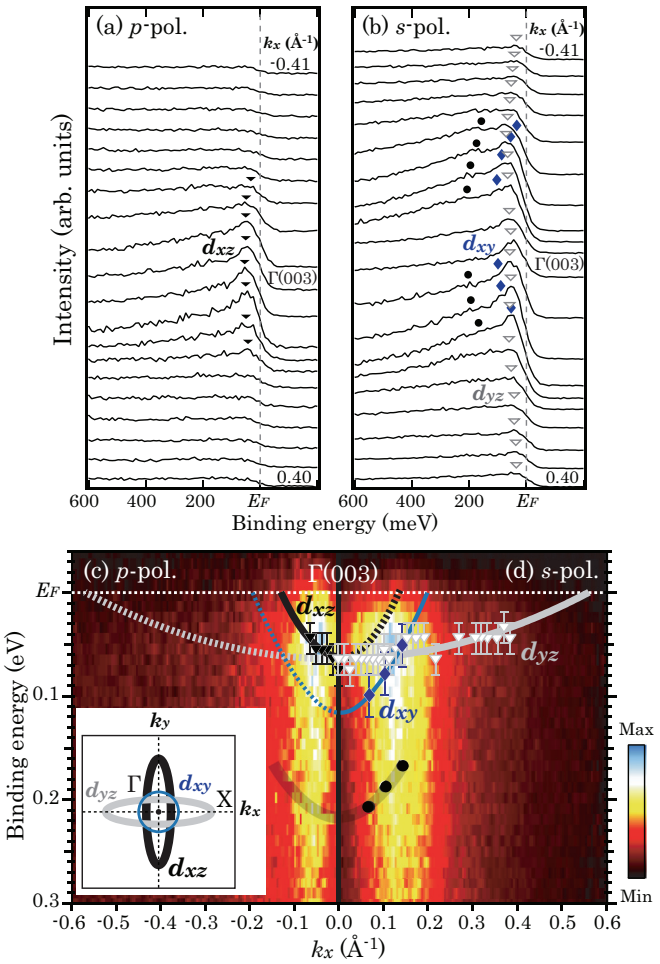

FIG. 4. (Color online) Summary of subbands for the metallic states at Γ(003) for the 4000 L H-dosed sample ($T = 80$ K, $\theta = 0°$, $h\nu = 81$ eV). (a) and (b) are EDCs along the k_x direction with the integration of about 0.04 Å^{-1}. (c) and (d) are ARPES intensity data taken with p and s polarization, respectively. The peak positions of d_{xz} (black triangle), d_{yz} (gray triangle), d_{xy} (blue diamond), and hump structure (black circle) are indicated. The inset shows the schematics of the Fermi surface map in the surface Brillouin zone.

summarized in Table I. Since only d_{xz} in Ti 3d t_{2g} can be observed with p-polarized light ($A_x + A_z$) in our experimental geometry, the dispersive feature in Fig. 4(a) is assigned to the d_{xz} band. The drop of the photoemission intensity from the d_{xz} band at Γ(003) in Figs. 3(a) and 3(c) and Figs. 4(a) and 4(c) is understood from the existence of the yz mirror plane at the normal emission geometry, where emissions from d_{xz} by A_z disappear and emissions by A_x are obtained. Similarly, d_{xy} and d_{yz} in Ti 3d t_{2g} can be observed with s-polarized light (A_y). A peak observed at Γ(003) can emerge from the d_{yz} orbital. Thus, a rather flat band at $E_B < 60$ meV in Fig. 4(b) is attributed to the d_{yz} band. On the other hand, a significant drop of the intensities of the bands at $E_B < 120$ meV and $E_B \sim 200$ meV indicates that they have the d_{xy} symmetry.

Based on these symmetry arguments, the dispersion curves of the metallic Ti 3d bands are summarized in Figs. 4(c) and 4(d). The Ti 3d_{xz} and 3d_{yz} bands have the band bottom at $E_B = 60 \pm 15$ meV and effective mass of $m_x^* \sim 1.8$ m$_e$ and $m_x^* \sim 22$ m$_e$, respectively, along the k_x direction (m$_e$ is the free electron mass). Although the spectral tail of the MS peak prevents from the accurate determination of the Ti 3d_{xy} band dispersion curve, it may have the band bottom at $E_B \sim 120$ meV with $m_x^* \sim 1.5$ m$_e$ as judged from the spectral feature in Fig. 4(b). The intensities of the hump states at $E_B \sim 200$ meV become small at $|k_x| > 0.2$ Å^{-1}, where the edges of the dispersion curve of the d_{xy} band cross the Fermi level. Thus, the hump states at $E_B \sim 200$ meV will likely be assigned to the incoherent peak of the Ti 3d_{xy} band enhanced by the polaronic or plasmonic interactions.[15,17,30] The energy separation between the d_{xy} peaks at $E_B < 120$ meV and incoherent peak at $E_B \sim 200$ meV in Fig. 4(b) is close to the separation measured on a recent temperature-dependent ARPES study on STO, into which electrons are induced by annealing the STO in the ultrahigh vacuum.[15] The presence of the d_{xy} band at higher binding energy than the d_{xz} and d_{yz} bands is also supported by the polarization dependence of the MS as observed in Fig. 2(b). The small intensity ratio of the MS ($I^p/I^s < 1$) precludes the case where the Ti 3d bands are triply degenerated and isotropic ($I^p/I^s \sim 2$). The d_{xy} band at higher binding energy would be less influenced by the smearing-out effect of density of state near the Fermi level by the Fermi-Dirac distribution. This may also contribute to the small intensity ratio of the MS.

The energy separation of the d_{xy} band from doubly degenerate d_{xz} and d_{yz} at Γ(003) can be explained by the electron-confinement effect in the surface-vertical direction[6] and/or by lowering of the crystal symmetry induced by the phase transition at the low temperature ($\lesssim$105 K).[15,31] Theoretical calculations predict that the d_{xy} band should energetically be lifted up from the d_{xz} and d_{yz} bands in STO with the low crystal symmetry,[31] while the experimentally verified band structure[15] is opposite to the theoretical prediction. Band bending (~200 meV) by hydrogen adsorption on the STO surface[8] rather supports the electron-confinement model than the lowering-of-symmetry model. Based on the energy positions of the Ti 3d t_{2g} bands, a thickness of the confinement layer at the energy, where electrons in the d_{xz} and d_{yz} states are confined, is estimated to be 2.1 nm by a triangular-potential approximation.[32] The estimated thickness is close to the effective thickness of previous studies for confined 2D electron systems on STO surfaces (1.4 ~ 5 nm).[6,7]

Concerning the IGS at $E_B \sim 1.3$ eV, it shows no dependence on either incident light polarizations or k_x (emission angles). Since the IGS energetically locates between the Ti 3d

TABLE I. A list of s, p, and d orbitals which have nonzero matrix elements against the vector potentials listed on the left, and have final states with even parities in the mirror planes at the top. The parities of orbitals with respect to the mirror plane are written inside the parentheses. It is of note that, in the present measurement geometry, p-polarized light excites electronic states in the A_x and A_z rows, while s-polarized light in the A_y row.

	xz mirror plane	yz mirror plane	normal emission
A_x	s, p_x, d_{xz} (even)	p_x, d_{xy}, d_{xz} (odd)	p_x, d_{xz}
A_y	p_y, d_{xy}, d_{yz} (odd)	s, p_y, d_{yz} (even)	p_y, d_{yz}
A_z	s, p_z, d_{xz} (even)	s, p_z, d_{yz} (even)	s, p_z

and O 2p bands, it may have contributions from the Ti 3d or O 2p states, or it may result from the Ti 3d–O 2p hybridized states. Table I shows that emissions from the p orbitals are independent on the mirror planes and are not weakened even at the normal emission. Thus, the IGS is mainly composed of the O 2p orbitals. The isotropic nature likely originates from the six O 2p–Ti 3d bonding coordinations along the three different orthogonal axes. The origin of the IGS has been argued by various models; it has been attributed to a locally screened incoherent state of the Ti 3d–O 2p band,[33] a precursor of the "lower-Hubbard band" of the d^1 insulator,[34] chemical disorder,[13] and the polaron effect.[35] Identification of the O 2p nature for the IGS on the well-defined surface rather favors the locally screening Ti 3d–O 2p band model.[33]

From the band dispersion plots in Fig. 4, Fermi surfaces of the metallic H/STO surface are inferred as shown in the inset. The Ti $3d_{xz}$ and d_{yz} bands have oval Fermi surfaces with the long axes along the k_x and k_y directions, respectively, while the Ti $3d_{xy}$ band has an isotropic Fermi circle. Within the electron confinement model, the 2D electron density n_{2D} is estimated as $n_{2D} \approx 3.9 \times 10^{14}$ cm^{-2}, which corresponds to 0.54 electrons in a surface unit cell (1.52×10^{-15} cm^2). The value is similar to those of the partially filled Ti 3d band reported on the cleaved STO(001) surfaces.[6,7] In our previous paper,[8] the n_{2D} on the H/STO surface prepared by the 1350 L H-dosage was estimated to be $n_{2D} \approx 6 \times 10^{13}$ cm^{-2} at 20 K based on the assumption of a single metallic band. The three subband structures revealed in this study reevaluate n_{2D} on the 1350 L H-dosed STO surface to be $n_{2D} \approx 3.1 \times 10^{14}$ cm^{-2}.

To study the adsorption site of the hydrogen atoms and to evaluate a ratio between numbers of electrons filling the Ti 3d t_{2g} bands and the adsorbed hydrogen atoms, core-level photoemission measurements were carried out on the clean and the hydrogen adsorbed STO(001) surfaces (Fig. 5). The multiple doublets and shoulders at high binding-energy side of the O 1s and Sr 3d spectra were observed on the clean

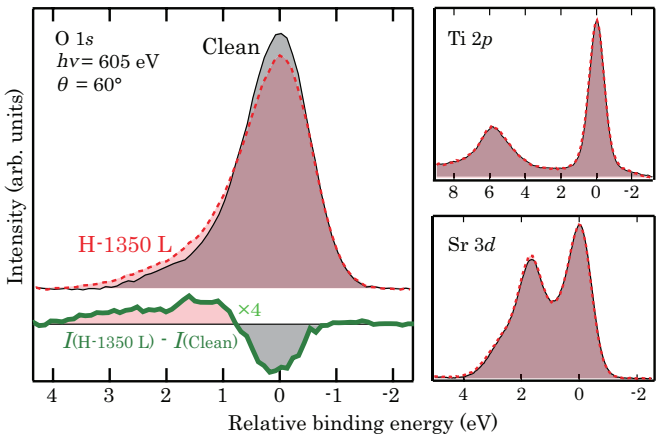

FIG. 5. (Color online) Core-level spectra of the clean (black solid) and 1350 L H-dosed STO surfaces (red dots) taken at $h\nu = 605$ eV and $\theta = 60°$. All spectra are taken with p polarization at 300 K. In order to evaluate the change in the line shape of the spectra, all the peak shifts caused by hydrogen adsorption were calibrated, and the intensities were normalized with their peak areas. The difference plot (green solid) shows the increase of the shoulder at the higher binding-energy side of the O 1s peak.

STO(001) surface, indicating the segregation of Sr oxides at the TiO_2-terminated surface.[36,37] By the 1350 L hydrogen dosage, the core-level peak of O 1s shows a discernible variation, while those of Ti 2p and Sr 3d show negligibly small changes. These results show that metallization is induced by hydrogen adsorption on the oxygen site, and segregated Sr atoms on the surface do not play an important role for metallization. In the O 1s spectra, the main peak intensity decreases and, at the same time, a spectral shoulder is enhanced at ~1.5 eV higher binding energy than the main peak. Since the emission from the O-H species on oxide surfaces usually appears at ~1.5 eV higher binding energy than that from oxygen in bulk oxide, the shoulder structure is attributed to O-H.[18,38,39] The area of the O-H feature corresponds to about 5.1% of the total area of the O 1s peak. The hydrogen coverage can be quantitatively evaluated from the photoemission intensity through the following equation:[40,41]

$$I = C \sum_{j=1}^{\infty} N_j \exp\left(-\frac{t_j}{\lambda \cos\theta}\right). \quad (3)$$

The constant C depends on the spectrometer efficiency, asymmetry parameter, photon flux, and photoionization cross section. N_j and t_j are the atomic density and the depth of the jth layer from the surface, respectively. The peak intensity I is a sum of the photoelectrons from the oxygen atoms located over the layers. The inelastic mean-free path (λ) is $\lambda = 5.75$ Å as estimated from the empirical formulation by Tanuma, Penn, and Powell (TPP-2M).[42] Under the assumption that the hydrogen atoms adsorb only at the oxygen atoms on the topmost TiO_2 layer, the number of hydrogen atoms on the surface is evaluated to be $0.8 \sim 1.1 \times 10^{14}$ cm^{-2} (or $0.12 \sim 0.17$ atoms per unit cell) at 300 K. When one assumes that each hydrogen atom provides one electron to the STO surface, the 2D electron density is estimated as $n_{2D} \sim 1 \times 10^{14}$ cm^{-2}, which is the same order of magnitude as the 2D electron density estimated from the Fermi surface. The simple estimation indicates that there is likely a good correlation between a number of hydrogen atoms adsorbed on the surface and that of electrons doped into the unoccupied Ti 3d band.

IV. CONCLUSIONS

Details of the electronic structure of the metallic band on the hydrogen-adsorbed STO(001) surface are revealed by the valence band and core-level photoemission spectroscopy study with polarized light. With the symmetric arguments, the H-induced peaks in the valence band region are attributed to σ(O-H) along the out-of-plane direction, the metallic states mainly composed of the Ti 3d t_{2g} components, and the IGS mainly composed of O 2p orbitals. Furthermore the state at 3 eV is also the H-induced one, which shows strong polarization dependence. The electrons at the MS partially fill in the Ti $3d_{xy}$ band and the doubly degenerate Ti $3d_{xz}$ and Ti $3d_{yz}$ bands. On the basis of the band bending effect by hydrogen adsorption on STO and the appearance of the incoherent peak at the MS, realization of the 2DEL phase on the H/STO surface is suggested.

ACKNOWLEDGMENTS

H. Kumigashira, M. Lippmaa, S. Kawasaki, S. Kitagawa, and Y. Ishida, T. Yoshida, and K. Yoshimatsu are gratefully appreciated for their warm support during the experiment and for the valuable discussions. This work was performed by using facilities of the Synchrotron Soleil, France, and Synchrotron Radiation Research Organization, the University of Tokyo (Proposal No. 7401 for 2009–2011 and Proposal No. 2011A7415). This work was supported by PICS/CNRS and by JSPS (KAKENHI 23560020).

*imatsuda@issp.u-tokyo.ac.jp

[1] A. Ohtomo and H. Y. Hwang, Nature (London) **427**, 423 (2004).

[2] M. Basletic, J.-L. Maurice, C. Carrétéro, G. Herranz, O. Copie, M. Bibes, É. Jacquet, K. Bouzehouane, S. Fusil, and A. Barthélémy, Nat. Mater. **7**, 621 (2008).

[3] W. Siemons, G. Koster, H. Yamamoto, W. A. Harrison, G. Lucovsky, T. H. Geballe, D. H. A. Blank, and M. R. Beasley, Phys. Rev. Lett. **98**, 196802 (2007).

[4] M. Breitschaft, V. Tinkl, N. Pavlenko, S. Paetel, C. Richter, J. R. Kirtley, Y. C. Liao, G. Hammerl, V. Eyert, T. Kopp *et al.*, Phys. Rev. B **81**, 153414 (2010).

[5] A. Brinkman, M. Huijben, M. van Zalk, J. Huijben, U. Zeitler, J. C. Maan, W. G. van der Wiel, G. Rijnders, D. H. A. Blank, and H. Hilgenkamp, Nat. Mater. **6**, 493 (2007).

[6] A. F. Santander-Syro, O. Copie, T. Kondo, F. Fortuna, S. Pailhès, R. Weht, X. G. Qiu, F. Bertran, A. Nicolaou, A. Taleb-Ibrahimi *et al.*, Nature (London) **469**, 189 (2011).

[7] W. Meevasana, P. D. C. King, R. H. He, S.-K. Mo, M. Hashimoto, A. Tamai, P. Songsiriritthigul, F. Baumberger, and Z.-X. Shen, Nat. Mater. **10**, 114 (2011).

[8] M. D'Angelo, R. Yukawa, K. Ozawa, S. Yamamoto, T. Hirahara, S. Hasegawa, M. G. Silly, F. Sirotti, and I. Matsuda, Phys. Rev. Lett. **108**, 116802 (2012).

[9] F. Polack, M. Silly, C. Chauvet, B. Lagarde, N. Bergeard, M. Izquierdo, O. Chubar, D. Krizmancic, M. Ribbens, J.-P. Duval *et al.*, AIP Conf. Proc. **1234**, 185 (2010).

[10] N. Bergeard, M. G. Silly, D. Krizmancic, C. Chauvet, M. Guzzo, J. P. Ricaud, M. Izquierdo, L. Stebel, P. Pittana, R. Sergo *et al.*, J. Synchrotron Radiat. **18**, 245 (2011).

[11] M. Ogawa, S. Yamamoto, Y. Kousa, F. Nakamura, R. Yukawa, A. Fukushima, A. Harasawa, H. Kondoh, Y. Tanaka, A. Kakizaki *et al.*, Rev. Sci. Instrum. **83**, 023109 (2012).

[12] T. Nishimura, A. Ikeda, H. Namba, T. Morishita, and Y. Kido, Surf. Sci. **421**, 273 (1999).

[13] D. D. Sarma, S. R. Barman, H. Kajueter, and G. Kotliar, Europhys. Lett. **36**, 307 (1996).

[14] Y. Haruyama, S. Kodaira, Y. Aiura, H. Bando, Y. Nishihara, T. Maruyama, Y. Sakisaka, and H. Kato, Phys. Rev. B **53**, 8032 (1996).

[15] Y. J. Chang, A. Bostwick, Y. S. Kim, K. Horn, and E. Rotenberg, Phys. Rev. B **81**, 235109 (2010).

[16] N. B. Brookes, F. M. Quinn, and G. Thornton, Phys. Scr. **36**, 711 (1987).

[17] F. Gervais, J.-L. Servoin, A. Baratoff, J. G. Bednorz, and G. Binnig, Phys. Rev. B **47**, 8187 (1993).

[18] S. Ferrer and G. A. Somorjai, Surf. Sci. **94**, 41 (1980).

[19] Y. Aiura, Y. Nishihara, Y. Haruyama, T. Komeda, S. Kodaira, Y. Sakisaka, T. Maruyama, and H. Kato, Phys. B (Amsterdam) **194-196**, 1215 (1994).

[20] Y. Aiura, I. Hase, H. Bando, T. Yasue, T. Saitoh, and D. S. Dessau, Surf. Sci. **515**, 61 (2002).

[21] S. Hüfner, *Photoelectron Spectroscopy* (Springer, Berlin, 1995).

[22] M. Guzzo, G. Lani, F. Sottile, P. Romaniello, M. Gatti, J. J. Kas, J. J. Rehr, M. G. Silly, F. Sirotti, and L. Reining, Phys. Rev. Lett. **107**, 166401 (2011).

[23] M. Guzzo, J. J. Kas, F. Sottile, M. G. Silly, F. Sirotti, J. J. Rehr, and L. Reining, Eur. Phys. J. B **85**, 324 (2012).

[24] W. Meevasana, X. J. Zhou, S. Sahrakorpi, W. S. Lee, W. L. Yang, K. Tanaka, N. Mannella, T. Yoshida, D. H. Lu, Y. L. Chen *et al.*, Phys. Rev. B **75**, 174506 (2007).

[25] S. L. Weng, E. W. Plummer, and T. Gustafsson, Phys. Rev. B **18**, 1718 (1978).

[26] F. Lin, S. Wang, F. Zheng, G. Zhou, J. Wu, B.-L. Gu, and W. Duan, Phys. Rev. B **79**, 035311 (2009).

[27] E. D. Hansen, T. Miller, and T.-C. Chiang, Phys. Rev. B **55**, 1871 (1997).

[28] T. Miller, W. E. McMahon, and T.-C. Chiang, Phys. Rev. Lett. **77**, 1167 (1996).

[29] H. J. Levinson, E. W. Plummer, and P. J. Feibelman, Phys. Rev. Lett. **43**, 952 (1979).

[30] J. L. M. van Mechelen, D. van der Marel, C. Grimaldi, A. B. Kuzmenko, N. P. Armitage, N. Reyren, H. Hagemann, and I. I. Mazin, Phys. Rev. Lett. **100**, 226403 (2008).

[31] L. F. Mattheiss, Phys. Rev. B **6**, 4740 (1972).

[32] To calculate the thickness of the confinement layer, the depth and the width of the triangular potential well are adjusted so as to reproduce the energy positions of the d_{xy} band and the doubly degenerated d_{xz} and d_{yz} bands at the Γ point. In addition, the effective mass of $m_z^* = 1.8\ \mathrm{m}_e$ for the d_{xz} and d_{yz} bands is applied. For details of the triangular potential well approximation, see J. H. Davies, *The Physics of Low-Dimensional Semiconductors: An Introduction* (Cambridge University Press, New York, 1998).

[33] Y. Ishida, R. Eguchi, M. Matsunami, K. Horiba, M. Taguchi, A. Chainani, Y. Senba, H. Ohashi, H. Ohta, and S. Shin, Phys. Rev. Lett. **100**, 056401 (2008).

[34] Y. Tokura, Y. Taguchi, Y. Okada, Y. Fujishima, T. Arima, K. Kumagai, and Y. Iye, Phys. Rev. Lett. **70**, 2126 (1993).

[35] A. Fujimori, A. E. Bocquet, K. Morikawa, K. Kobayashi, T. Saitoh, Y. Tokura, I. Hase, and M. Onoda, J. Phys. Chem. Solids **57**, 1379 (1996).

[36] K. Szot and W. Speier, Phys. Rev. B **60**, 5909 (1999).

[37] D. Kobayashi, H. Kumigashira, M. Oshima, T. Ohnishi, M. Lippmaa, K. Ono, M. Kawasaki, and H. Koinuma, J. Appl. Phys. **96**, 7183 (2004).

[38] G. Ketteler, S. Yamamoto, H. Bluhm, K. Andersson, D. E. Starr, D. F. Ogletree, H. Ogasawara, A. Nilsson, and M. Salmeron, J. Phys. Chem. C **111**, 8278 (2007).

[39] M. Knapp, D. Crihan, A. P. Seitsonen, E. Lundgren, A. Resta, and J. N. Andersen, J. Phys. Chem. C **111**, 5363 (2007).

[40] S. Yamamoto, T. Kendelewicz, J. T. Newberg, G. Ketteler, D. E. Starr, E. R. Mysak, K. J. Andersson, H. Ogasawara, H. Bluhm, M. Salmeron *et al.*, J. Phys. Chem. C **114**, 2256 (2010).

[41] P. Liu, T. Kendelewicz, G. E. Brown, and G. A. Parks, Surf. Sci. **412–413**, 287 (1998).

[42] S. Tanuma, C. J. Powell, and D. R. Penn, Surf. Interface Anal. **21**, 165 (1994).